**Rational Design Calculation of Surface Acoustic Wave Gas Sensor**

Mohammad Yaghoub Abdollahzadeh Jamalabadi
Chabahar Maritime University

**Abstract:**

The high temperature of surface acoustic wave resonator at specific frequencies is an important challenge for electronic designers. Various modifications of the cooling in ZnO based sensitive element for the two-port surface acoustic wave sensor (SAW) design were considered. The effect of microchannel for cooling in SAW sensor characteristics was investigated by finite element simulation method. Obtained versatile flexible multiparameter model allowed the evaluation of performance parameters. The optimal parameters for SAW sensor design could be estimated by the proposed approach.

**Keywords** Surface acoustic waves ;thermal design ;gas sensor ;heat removal ;MEMS

# 1 Introduction

Surface Acoustic Wave (SAW) is a category of compressive (mechanical) waves. These types of waves require an elastic solid medium to transmit. [1] Piezoelectric materials (which are a kind of elastic solid) are commonly used to transmit these waves. Surface acoustic waves create an electric field in piezoelectric materials. It has the potential to be widely used in telecommunications and signal processing.

These days acoustic wave gadgets are generally applied in numerous modern and logical fields running from cell phones and remote correspondence, weight and consistency sensors to novel biosensors for DNA recognition. Significant points of interest of surface acoustic wave (SAW) sensors include: single sided planar structure, capacity to communicate straightforwardly with the detecting medium, high affectability, low hysteresis, little size, direct recurrence yield flag and low force utilization. Expansion of mass influences not just recurrence yet additionally stage and greatness. This component gives progressively exact estimation of analyte focus.

Surface acoustic filters are used to process electrical signals. A simple type of these filters consists of two interdigital transducers (IDTs) mounted on a piezoelectric substrate. One of these transducers acts as a transmitter in the presence of an electrical voltage of mechanical (acoustic) waves. The other one acts as the receiver of these waves and returns the incoming wave to an electronic signal.

A surface acoustic wave (SAW) is an acoustic wave multiplying along the outside of a solid material. Its adequacy decays rapidly, consistently exponentially, with the significance of the material. SAWs are featured in various sorts of electronic parts, including channels, oscillators, and sensors. SAW contraptions conventionally use terminals on a piezoelectric material to change over an electric sign to a SAW, and back again.

Surface acoustic wave propagation in piezoelectric materials first by Lord Riley Introduced in 1885 [1] White and Voltmer were introduced in 1965 [2] Types of sound waves that propagate along the surface of a material. This The wave is produced by the shoulder electrodes. The metal electrodes are coated on a piezoelectric material at equal distances. When a sinusoidal wave with a specified periodicity for shoulder- A vibration is generated at the substrate surface and an acoustic wave, Perpendicular to the electrodes.

At the present time, investigate the resonation frequencies of a SAW gas sensor. The sensor contains an interdigitated transducer (IDT) scratched onto a piezoelectric LiNbO3 (lithium niobate) substrate and made sure about with a thin polyisobutylene (PIB) film. The mass of the PIB film augments as PIB explicitly adsorbs CH2Cl2 (dichloromethane, DCM) from air. This causes a move in resonation which to some degree cuts down the resonation repeat for a comparative SAW mode.

Examination of novel touchy materials, their combination techniques for cutting edge sensors is a genuine issue and consistently did [1]. Among confused and costly customary manufacture procedures such low-temperature amalgamation strategies as aqueous strategy is appropriate for nanostructures amalgamation nearly on any substrates incorporate singlecrystal [2]. ZnO nanorods have been utilized as bioor gas touchy component of SAW sensors emphatically impacting on both acoustic and electric impedance of SAW structure, because of goliath viable surface territory what's more, solid holding destinations and along these lines permits improving of affectability of such gadgets [3]. The systematic demonstrating of the plane harmonic surface wave engendering process in an isotropic versatile half-space with pole nanostructures on a surface (Fig. 1, a) for deciding of the engendering speed of surface waves at given geometric parameters of the pole nanostructures is introduced in [4]. This model disentangles the advancement of ZnO nanorods SAW sensors and examination of the outcomes. The reenactment of ZnO nanowire (Fig. 1, b) based gas sensor in COMSOL Multiphysics programming stage is introduced in [5]. Various thicknesses of ZnO middle of the road layer show diverse detecting execution in the wake of being presented to H2 gas.

This type of wave on the surface of matter The piezoelectric is propagated away from the electrodes in both their front and back directions. At surface waves, the wave is positioned and measured only in the wafer surface area A wavelength penetrates the depth. This means that this wave is one It has a very high energy density at its surface, hence the surface acoustic wave It's called small. Wave velocity in piezoelectric materials 10 More than the waves Is electromagnetic. Thus the transient wavelength in piezoelectric materials The small fold has a factor of $10^-5$ Is more than electromagnetic waves and can be considered as a compact device [3] Surface acoustic wave sensors are widespread today. Sensors Living bio-based can be a cheap alternative to High-cost biological sensors such as surface-resonant palmson resonators, Or radioimmunoassay testing methods for the detection of immunoflora test Be it All the methods mentioned have two major drawbacks: First, the high costs They have many and secondly are only sensitive to one type of particle or cell. Surface acoustic wave sensors are very popular because of their cheapness , But also have limitations, such as the initial reactivity with Specific antigens are only sensitive to one type of biological target particle, Secondly, the reactant layer is disposable and because of the reaction with the target particle, Can no longer be used.

Among the different types of microfluidic biosensors, Wave Acoustic Surface Technology (SAW) It has remarkable capabilities that are evident to the attention of lab-chip researchers -a-on-Lab Chip). SAW sensors are electronic devices in which surface acoustic waves with Applying a suitable electric field to a piezoelectric material is produced. This technology has wide applications in Has biological/chemical assays. LiNbO3 (lithium niobium) for growth and proliferation studies Materials and Methods: SAW sensors on piezoelectric substrate Cancer cells as well as evaluation of the effect of anticancer drugs on cell biochemical parameters, designed and fabricated Were. Based on TSAW, with two pairs of IDT transducers and for working on An approximate resonance frequency of 3.10 MHz is designed. Sensor response in the presence of empty cell culture solution, SW-48 cancer cells as well as cells Under the influence of albendazole, the analyzer network was measured. According to the results, the presence Suspended cells in the culture medium resulted in a change in the sensor response to the cell-free culture medium. also Clinging to cells by disrupting the acoustic wave velocity causes resonant frequency shifts Lower frequencies and shift to peak frequency in response to the drug applied to the attached cells. Higher frequencies. These changes are dependent on the elastic parameters and the mass of the cells shown on the sensor This enables the measurement of mass disturbances along the wave propagation path. Anti-cancer drugs block the proliferation of cells on the surface and therefore shift the frequency

Resonance decreases in drug-affected samples. Frequency shift value compared to the control sample that level It can also depend on the dose and potency of the drug coated. So SAW sensors as Free-Label Biosensors are applicable in drug resistance assays and diagnostic methods.

These types of sensors generally have two basic types of structure. Type one single It is a port, called a resonator. It's kind of just a set It has a transmitter electrode. But in addition to this transmitter electrode, also the reflective network There can trap a surface wave and form a cavity Vibrate and increase the surface acoustic wave effect. The second type The device is a dual-port, also called a delay line, as such It has two transmit and receive ports. At the receiving port one can wave Received and analyzed [6]. In liquid environments, Riley surface waves are a perpendicular displacement component The surface has a substrate. As the pressure waves lead to a sharp drop in the wave . For this reason, polarized waves are preferred horizontal shear Is. Because they are not elastically coupled to the ideal fluid and drop It does not cause wave reflection [7].

Horizontal shear modes can be operated using a steering wheel on The piezo substrate becomes a plum wave. In the waves of hail because of the existence of a layer Wave guidance is very sensitive to surface perturbations and high sensitivity To surface loading. Research has shown that to create a halo wave The sensitivity of LiTaO3 / ZnO and Quartz / ZnO is far greater than the structure SiO2 / LiTaO3 and SiO2 / Quartz [8]. Polymeric waveguide conduction has also been performed, but because of the property The viscosity of the polymers and consequently their high drop reduced overall efficiency he does. Metal oxides have a faster transmission speed than polymers. There will be more damping in the polymers as well It can dissipate until all energy is lost. A wave is a type of surface acoustic wave Includes a shear wave perpendicular to the propagation direction and tangent to the surface And is produced when a waveguide layer on the bed The piezoelectric is positioned and excited by the electric field Horizontal shear on the surface. The main requirement for publication The waveform is that the shear speed of the waveguide must be less than the speed The sound is at the bottom. Other surface waves can be type waves "Liqueur" produced by LiTaO3 substrates with specific angles, or one Surface "Black Skimming" wave produced by a single-layer quartz substrate The waveguide pointed out [9] Measuring the properties of liquids (eg viscosity and density) [10-12] As biosensor [13], [chemical sensor] [14] and test layers Composite [15] is used. One of the methods for detecting the sensor is the following Sensitive layers of graphene oxide layer as gases identification Chemical [16] is also mentioned.

## 2 Modeling

Figure 1 shows a sensible point of view on the gas sensor at this moment. The particle motion in a piezoelectric medium is based on elastic wave equation is calculated by

$$\rho\frac{\partial^2 u_i}{\partial t^2} = \frac{\partial T_{ij}}{\partial x_j} \tag{1}$$

where stress field

$$T_{ij} = s^E_{ijkl}S_{kl} + d_{ikl}E_k \tag{2}$$

In matrix form

$$T_{ij} = T_{11}T_{12}T_{13}T_{22}T_{23}T_{33} \tag{3}$$

Strain field

$$S_{ij} = (u_{i,j} + u_{j,i})/2, \tag{4}$$

In matrix form

$$S_{ij} = S_{11}S_{12}S_{13}S_{22}S_{23}S_{33} \tag{5}$$

Electric field

$$E_i = -\phi_{,i} \tag{6}$$

In matrix form

$$E_i = -\phi_{,1}\phi_{,2}\phi_{,3} \tag{7}$$

elastic constants

$$s^E_{ijkl} = \begin{bmatrix} s^E_{11} & s^E_{12} & s^E_{13} & 0 & 0 & 0 \\ s^E_{12} & s^E_{11} & s^E_{13} & 0 & 0 & 0 \\ s^E_{13} & s^E_{13} & s^E_{33} & 0 & 0 & 0 \\ 0 & 0 & 0 & s^E_{44} & 0 & 0 \\ 0 & 0 & 0 & 0 & s^E_{44} & 0 \\ 0 & 0 & 0 & 0 & 0 & s^E_{66} \end{bmatrix} \tag{8}$$

piezoelectric constants

$$d_{ijk} = \begin{bmatrix} 0 & 0 & 0 & 0 & d_{15} & 0 \\ 0 & 0 & 0 & d_{15} & 0 & 0 \\ d_{31} & d_{31} & d_{33} & 0 & 0 & 0 \end{bmatrix} \tag{9}$$

or stress field

$$T_{ij} = \begin{bmatrix} s^E_{11} & s^E_{12} & s^E_{13} & 0 & 0 & 0 \\ s^E_{12} & s^E_{11} & s^E_{13} & 0 & 0 & 0 \\ s^E_{13} & s^E_{13} & s^E_{33} & 0 & 0 & 0 \\ 0 & 0 & 0 & s^E_{44} & 0 & 0 \\ 0 & 0 & 0 & 0 & s^E_{44} & 0 \\ 0 & 0 & 0 & 0 & 0 & s^E_{66} \end{bmatrix} S_{kl} + \begin{bmatrix} 0 & 0 & 0 & 0 & d_{15} & 0 \\ 0 & 0 & 0 & d_{15} & 0 & 0 \\ d_{31} & d_{31} & d_{33} & 0 & 0 & 0 \end{bmatrix} E_k \tag{10}$$

since

$$\rho \frac{\partial^2 u_i}{\partial t^2} = s^E_{ijkl} \frac{\partial^2 u_k}{\partial x_j \partial x_l} + d_{ijk} \frac{\partial^2 \phi}{\partial x_j \partial x_k} \tag{11}$$

Electric field in a piezoelectric medium is calculated by the divergence of the electrical displacement vector D (must be equal to zero), where electric displacement

$$D_i = d_{ikl} S_{kl} + \varepsilon^T_{ik} E_k \tag{12}$$

dielectric permittivity constants

$$\varepsilon^T_{ik} = \varepsilon^T_{11}$$
$$0$$
$$0$$
$$0$$
$$\varepsilon^T_{22}$$
$$0$$
$$0$$
$$0$$
$$\varepsilon^T_{33}$$

(13)

electric displacement

$$D_i = \begin{bmatrix} 0 & 0 & 0 & 0 & d_{15} & 0 \\ 0 & 0 & 0 & d_{15} & 0 & 0 \\ d_{31} & d_{31} & d_{33} & 0 & 0 & 0 \end{bmatrix} T_{kl} + \varepsilon_{11}^T 000 \varepsilon_{22}^T 000 \varepsilon_{33}^T E_k \tag{14}$$

Electric field in a piezoelectric medium is calculated by

$$d_{jkl} \frac{\partial^2 u_k}{\partial x_j \partial x_l} = \varepsilon_{jk} \frac{\partial^2 \phi}{\partial x_j \partial x_k} \tag{15}$$

IDTs used in SAW contraptions may have a few undefined anodes, and each cathode can be around numerous occasions longer than it is wide. You can subsequently ignore the edge impacts and diminish the model geometry to the irregular unit cell showed up in Figure 2. The stature of this cell doesn't have to loosen up right to the base of the substrate anyway only a few frequencies down, with the objective that the SAW has about evaporated at as far as possible.

Thermal field is

$$\nabla^2 T + \frac{Q}{K} = \frac{1}{\kappa} \frac{\partial T}{\partial t} \tag{16}$$

| Parameter | Expression | Explanation |
|---|---|---|
| P | 1[atm] | Air pressure |
| T | $25[^oC]$ | Air temperature |
| $c_0$ | 100 | dichloromethane concentration in ppm |
| $c_{DCM,air}$ | $\frac{10^{-6} c_0 p}{R_{const} * T}$ | dichloromethane concentration in air |
| $M_{DCM}$ | 84.93 $[g/mol]$ | Molar mass of dichloromethane |
| K | $10^{1.4821}$ | polyisobutylene/air partition constant for dichloromethane |
| $\rho_{DCM,PIB}$ | $K M_{DCM} c_{DCM,air}$ | Mass concentration of dichloromethane in polyisobutylene |
| $\rho_{PIB}$ | 0.918 $[g/cm^3]$ | Density of polyisobutylene |
| $E_{PIB}$ | $10[GPa]$ | Young's modulus of polyisobutylene |
| $\nu_{PIB}$ | 0.48 | Poisson's ratio of polyisobutylene |
| $\epsilon_{PIB}$ | 2.2 | Relative permittivity of polyisobutylene |
| switch | 0 | Switch for adding dichloromethane density |
| $v_{Rayleigh}$ | $3488[m/s]$ | Rayleigh wave velocity |
| W | $4[\mu m]$ | Width of unit cell |
| $f_0$ | $\frac{v_{Rayleigh}}{W}$ | Estimated SAW frequency |
| $t_{PIB}$ | $0.5[\mu m]$ | polyisobutylene thickness |

Table 1: Table taken from

Set up the model using the predefined Piezoelectricity multiphysics interface. In 2D, a Plane Strain supposition that is used for the Solid Mechanics interface. From now on the out-of-plane strain part is zero. This should be a significant supposition, considering that the SAW is made in the plane of the model and along these lines any assortment in the out-of-plane heading can be seen as unimportant.

In order to portray the model, you need to apply assistant and electrical cutoff conditions. As one can acknowledge that the surface wave stops to exist inside a couple of frequencies from the surface, as far as possible is fixed. This maintains a zero fundamental expulsion anyway doesn't add to any basic reflection from as far as possible indeed into most of the substrate as long as we are watching surface waves and explicitly Rayleigh waves.

The anodes have a much higher electrical conductivity stood out from PIB and LiNbO3. Consequently, one can envision that all of the anodes ought to be isopotential. This is the explanation you don't need to show the spaces that include the anodes anyway can simply use appropriate breaking point conditions on all the outer furthest reaches of each terminal to show what kind of isopotential state it is in. The constraints of the left terminal is set to electrical ground, and those of the right terminal are given out to a Floating Potential with zero surface charge gathering. This mix of electrical breaking point conditions thinks about to an open circuit course of action, which is consistently fitting for recognizing applications.

Use discontinuous limit conditions to coordinate that the electric potential and movements are the identical along both vertical constraints of the geometry. While using discontinuous cutoff conditions, one needs to ensure that the work on as far as possible on the left of the unit cell and as far as possible on the benefit of the unit cell are unclear. This is practiced by first making the work on as far as possible on the left and a short time later using the Copy Edge feature to make definitely a similar work on as far as possible on the right. Each and every other cutoff are left to as far as possible conditions which are Free for the Solid Mechanics interface and Zero Charge for the Electrostatics interface, independently.

The substrate used in the reenactment is YZ-cut LiNbO3 with the going with properties (refered to in Ref. 2). The thickness of the PIB film is from [1]. The Poisson's extent is seen as 0.48, and the Young's modulus is set to 10 GPa. The adsorption of DCM gas is addressed as a slight augmentation of the general thickness of the PIB film as showed up in the going with enunciation. At the present time, use a parameter, switch, whose value can be either 0 or 1. This licenses to understand the model for two cases; once without the effect of adsorbed gas and once with the effect of the adsorbed DCM gas in PIB.

Right when the sensor is introduced to 100 ppm of DCM in air at ecological weight and room temperature, the "midway thickness" of DCM in the PIB film can be resolved from where $K = 10l.4821$ [1] is the air/PIB bundle coefficient for DCM, M is its molar mass, and c is its obsession in air. The DCM obsession, c in moles/m3 is enlisted using the Gas Law. Here c0 is the concentration in parts per million, p is the weight, T is the temperature, and R is the gas steady. Any effects of the DCM adsorption on the material properties other than the thickness are ignored.

Most of the material properties and components affecting them have been parameterized as showed up in Table 1. This adequately allows the model to be balanced for various materials and working conditions.

The usage of discontinuous breaking point condition proposes that the frequencies of interest identify with frequencies that are entire number divisions of the width of the geometry. The least SAW eigenmode has its recurrence equal to the width of the geometry, that is, 4 $\mu m$. Using this nearby the Rayleigh wave speed for the given piezoelectric substrate material, one can find a check of the resonation repeat of interest. The information can be used in the eigenfrequency solver, which makes it find the resonation frequencies close to this assessed number. At the present time, use a YZ-cut LiNbO3 whose Rayleigh wave speed ($v_R$) is around $3488 m/s$. This gives a check of the least SAW repeat ($f_0$) to be 872 MHz.

## 3 Results and Discussion

The antiresonance and resonation frequencies evaluate to around 850 MHz and 855$MHz$, separately. Figure 3 and Figure 4 show the looking at SAW modes. Figure 5 and Figure 6 show the electric potential scattering characteristics for these courses of action.

Introducing the sensor to a 100$ppm$ centralization of DCM in air prompts a resonation repeat move of around 200$Hz$ plummeting. This move is figured by evaluating the resonation repeat while including the thickness of adsorbed DCM to that of the PIB space.

Note that the computational work is indistinct in both these game plans. This surmises the general screw up of the repeat move resembles that of the resonation repeat itself. Right now, move is absolutely surveyed notwithstanding being several degrees more diminutive than the complete goof of the resonation repeat.

| without cooling | cooled | relative discrepancy percent between these values |
|---|---|---|
| 8.4903E8 | 8.4832E8 | 0.0836 |
| 8.5548E8 | 8.5253E8 | 0.3448 |
| 9.1857E8 | 9.1771E8 | 0.0936 |
| 9.3483E8 | 9.3526E8 | 0.0460 |
| 9.3516E8 | 9.3579E8 | 0.0674 |
| 9.7219E8 | 9.7125E8 | 0.0967 |

Table 2: Modes of solid $\lambda$ (Hz)

| Parameter | Value |
|---|---|
| lambda (Hz) | 4903E8 |
| Participation factor normalized, X-translation | 8. |
| Participation factor, normalized, Y-translation | 6.4974E-12 |
| Participation factor, normalized, Z-translation | 1.4404E-13 |
| Participation factor, normalized, Z-rotation | 2.8313E-10 |
| Effective modal mass, X-translation (kg) | 4.2216E-23 |
| Effective modal mass, Y-translation (kg) | 2.0747E-26 |
| Effective modal mass, Z-rotation (kg.m$^2$) | 8.0162E-20 |

Table 3: *lambda* (Hz)

Fig. 1 shows the SAW gas sensor, exhibiting the IDT anodes (in dim), the slim PIB film (light diminish), and the LiNbO3 substrate (diminish dim). For clarity, the estimations are unquestionably not to scale and the IDT shares less anodes than for all goals and reason devices. A cut of the geometry is removed to reveal the showed unit cell (in white).

Fig. 3 shows the Electric potential course at resonation, symmetric with respect to the point of convergence of each terminal.

Fig. 4 shows the geometry of the SAW unit cell used at the present time. A 500 nm PIB film covers two. The SAW is the rush of the double properties of longitudinal waves and shear waves. It is the coupling consequence of the S-waves and the P-waves. The molecule movement track is situated in the plane including the engendering course and the vertical strong surface. The size of the molecule adequacy is identified with the versatility of the materials and the

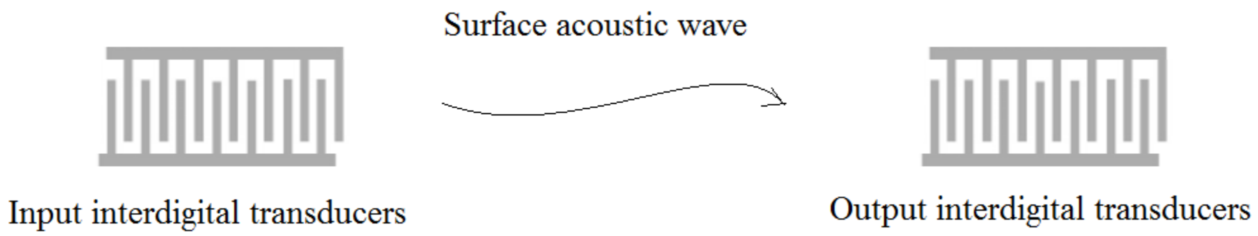


Figure 1: Input and output of SAW

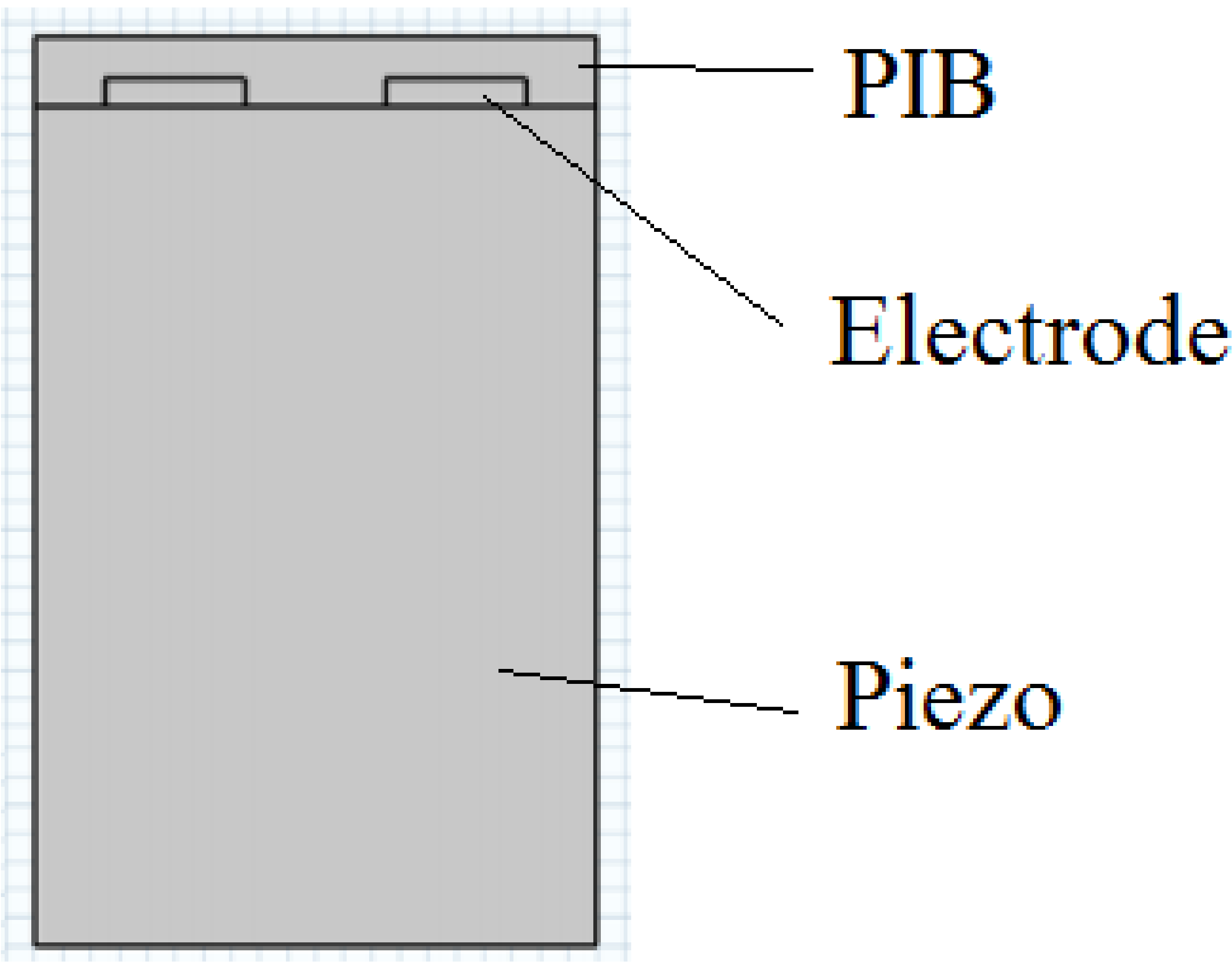


Figure 2: Geometry of the SAW

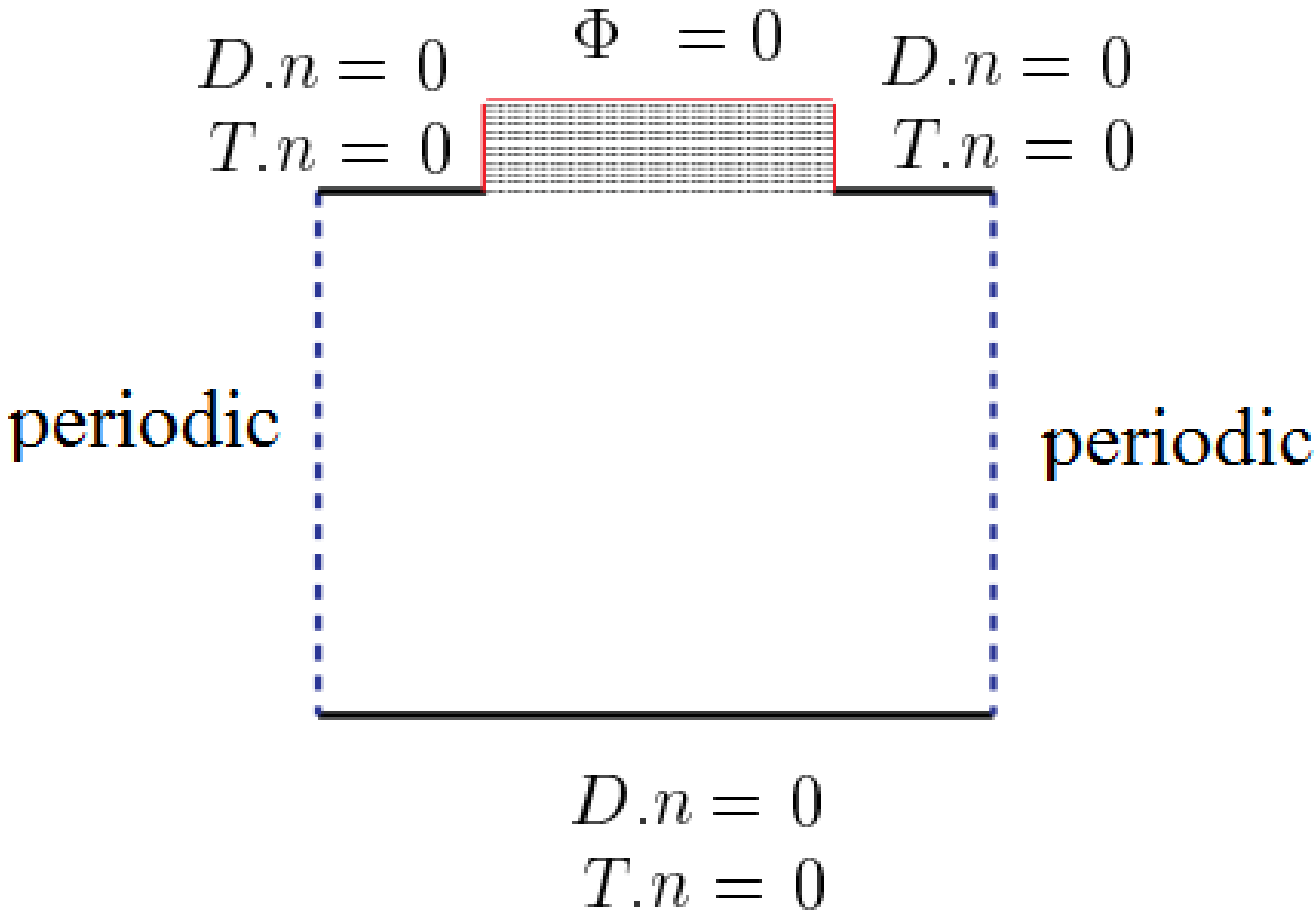


Figure 3: Typical geometry of the SAW unit cell and boundary condition

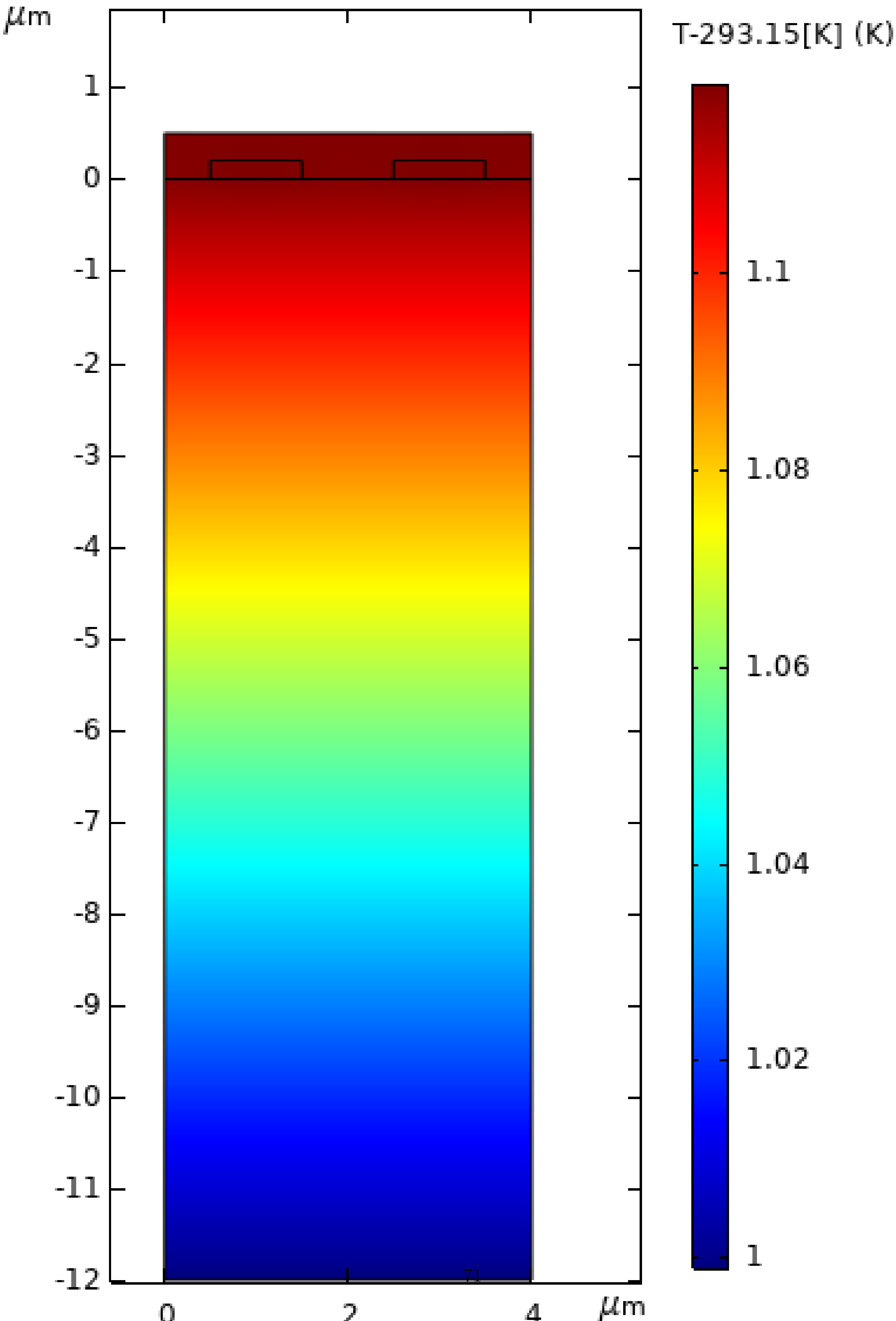
μm
1
0
-1
-2
-3
-4
-5
-6
-7
-8
-9
-10
-11
-12
0
2
4
μm
T-293.15[K] (K)
1.1
1.08
1.06
1.04
1.02
1

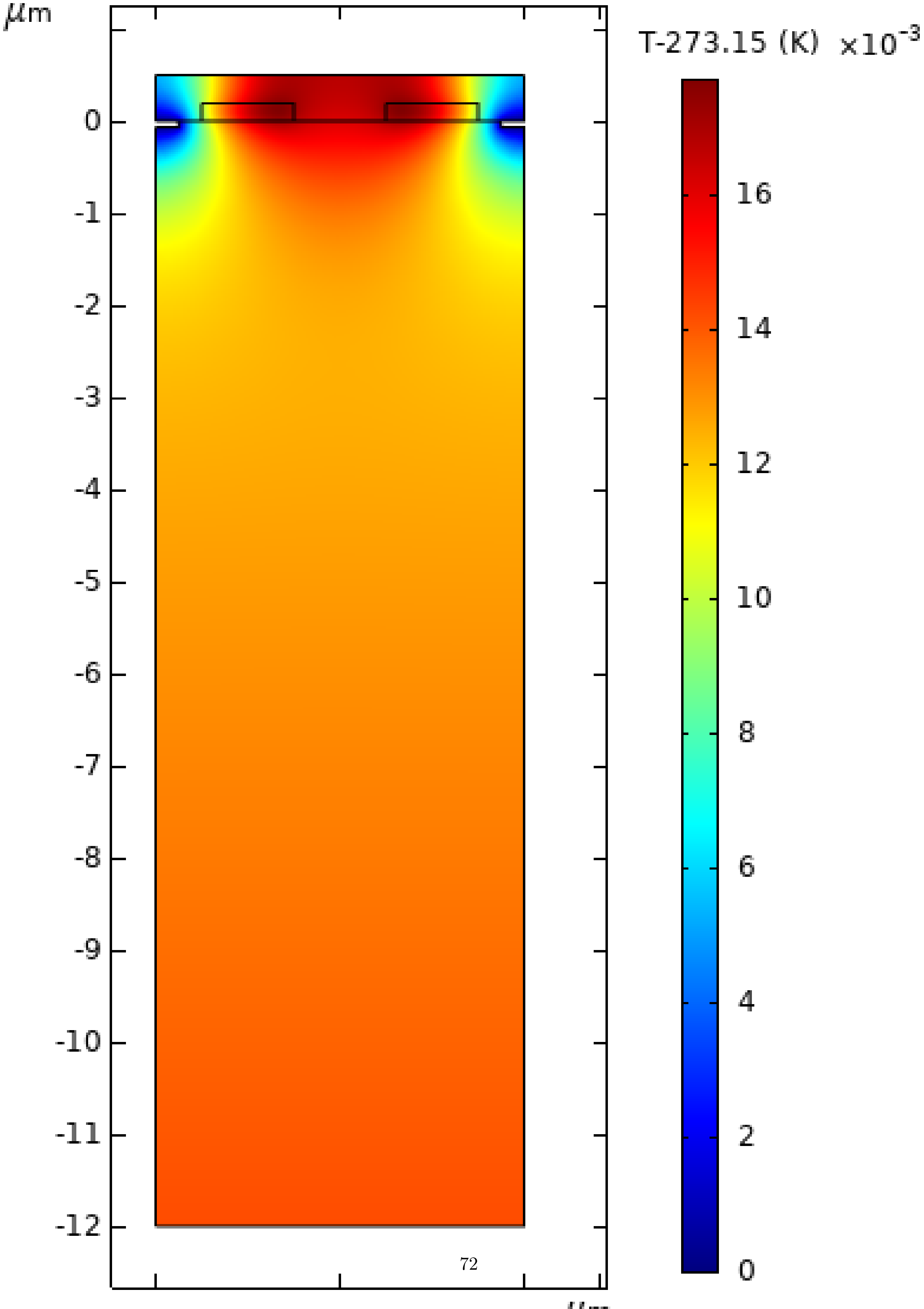
μm
0
-1
-2
-3
-4
-5
-6
-7
-8
-9
-10
-11
-12
T-273.15 (K) ×10$^{-3}$
16
14
12
10
8
6
4
2
0

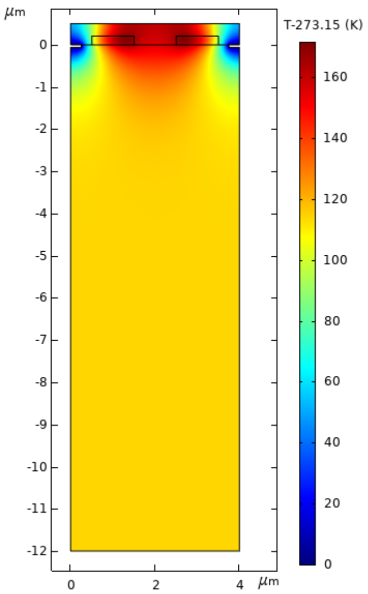


Figure 6: Temperature distribution in SAW with cooling at higher power

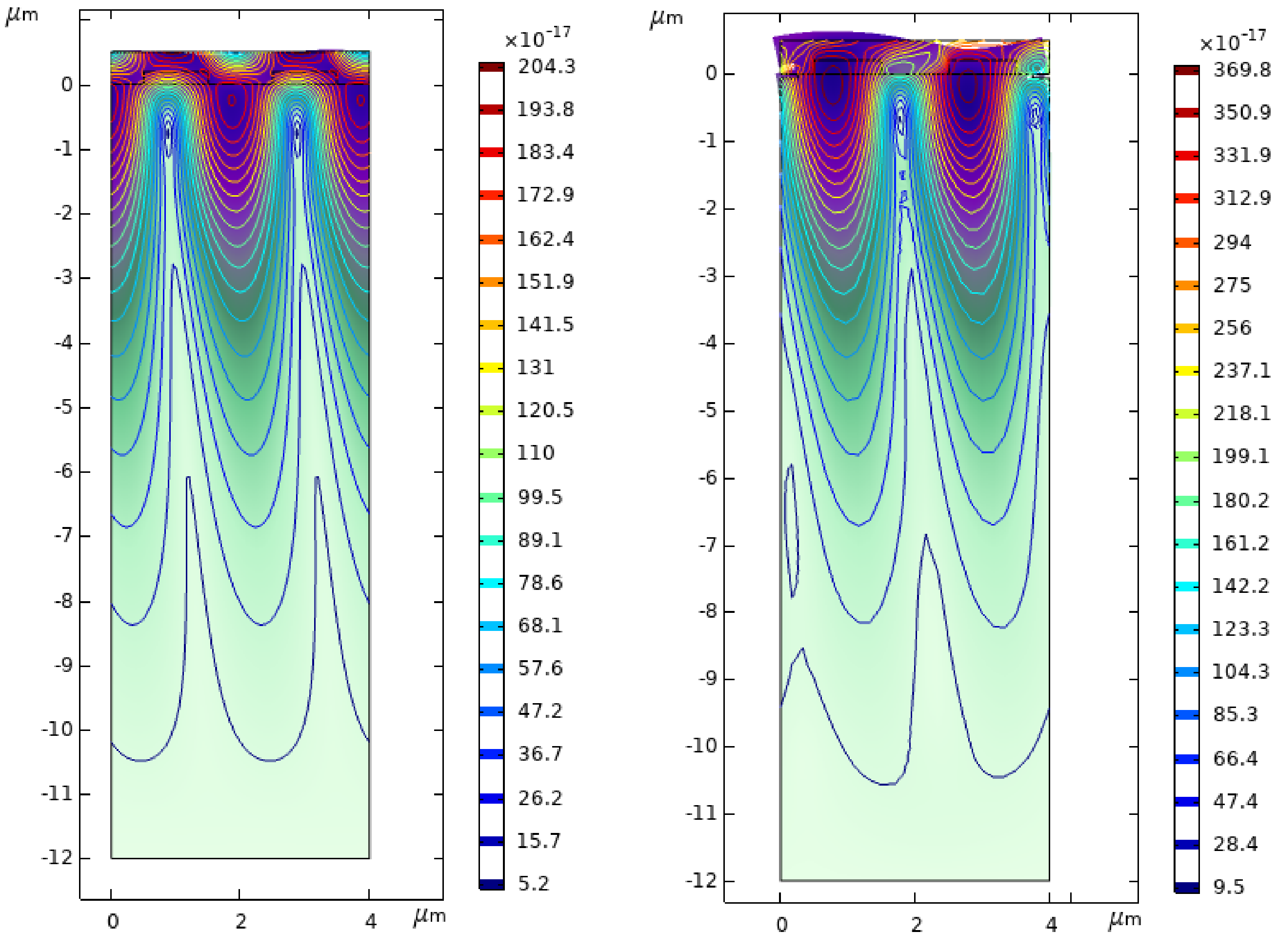

Figure 7: Mode 1 of solid mechanics.

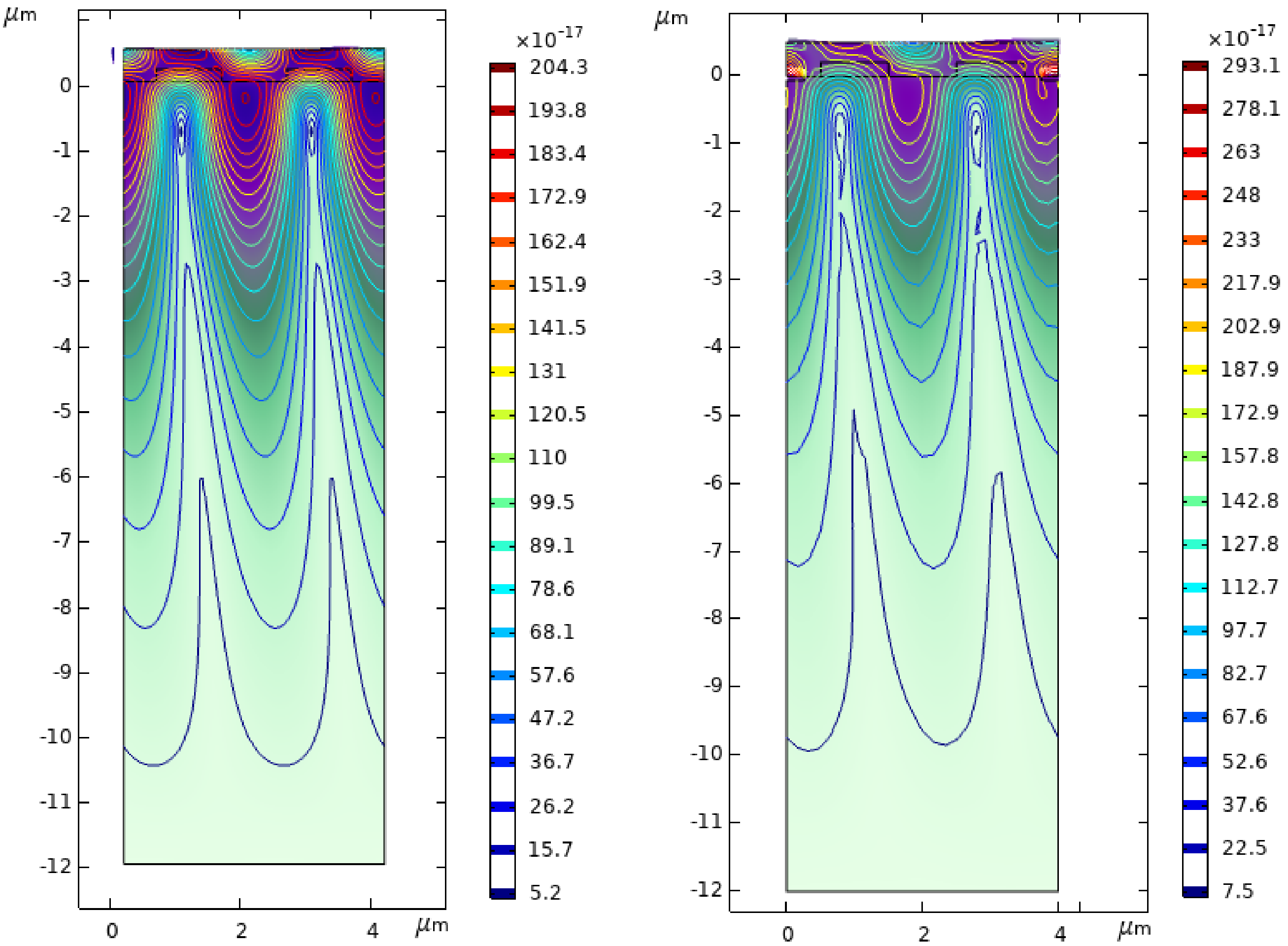


Figure 8: Mode 2 of solid mechanics.

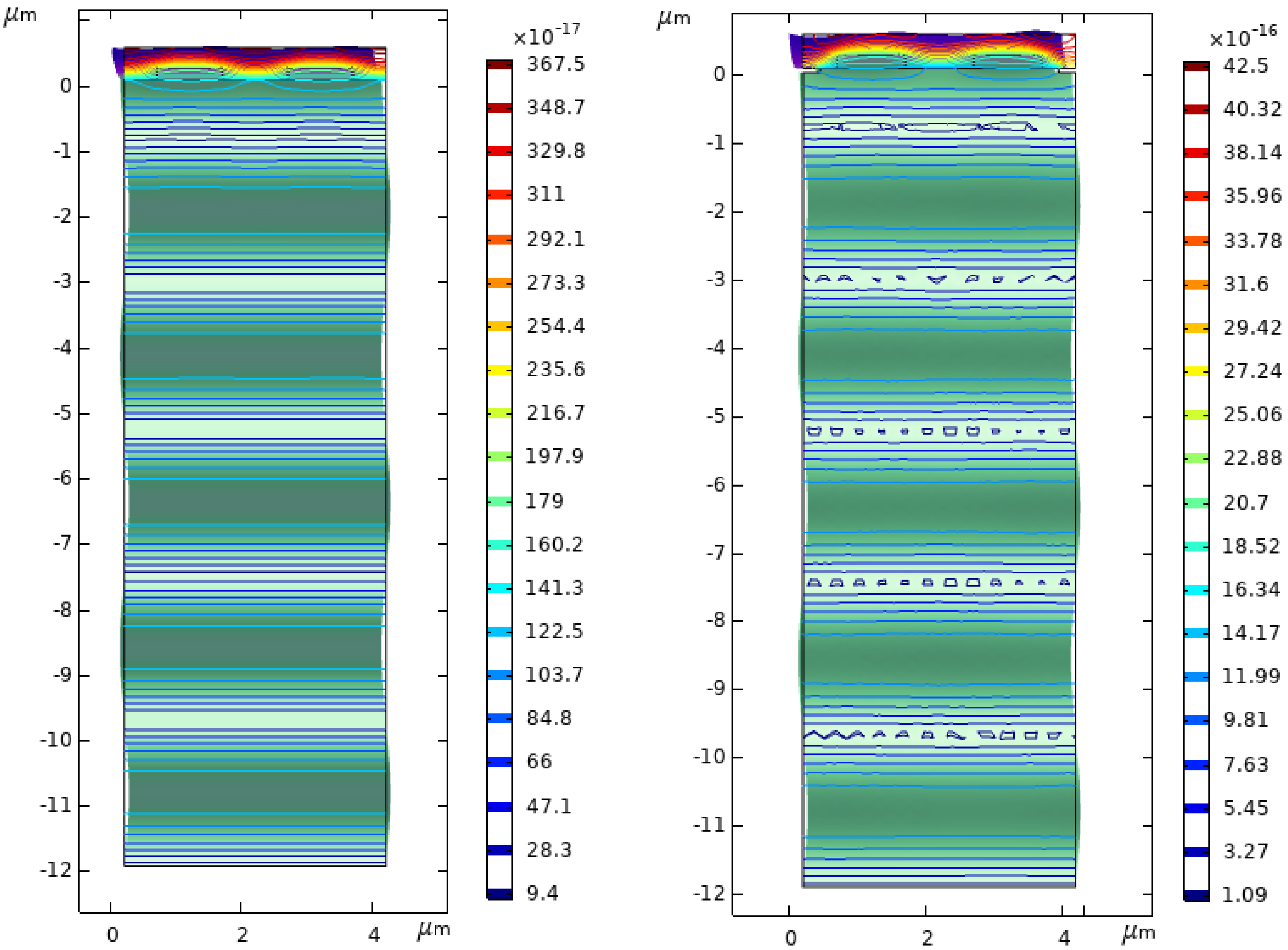


Figure 9: Mode 3 of solid mechanics.

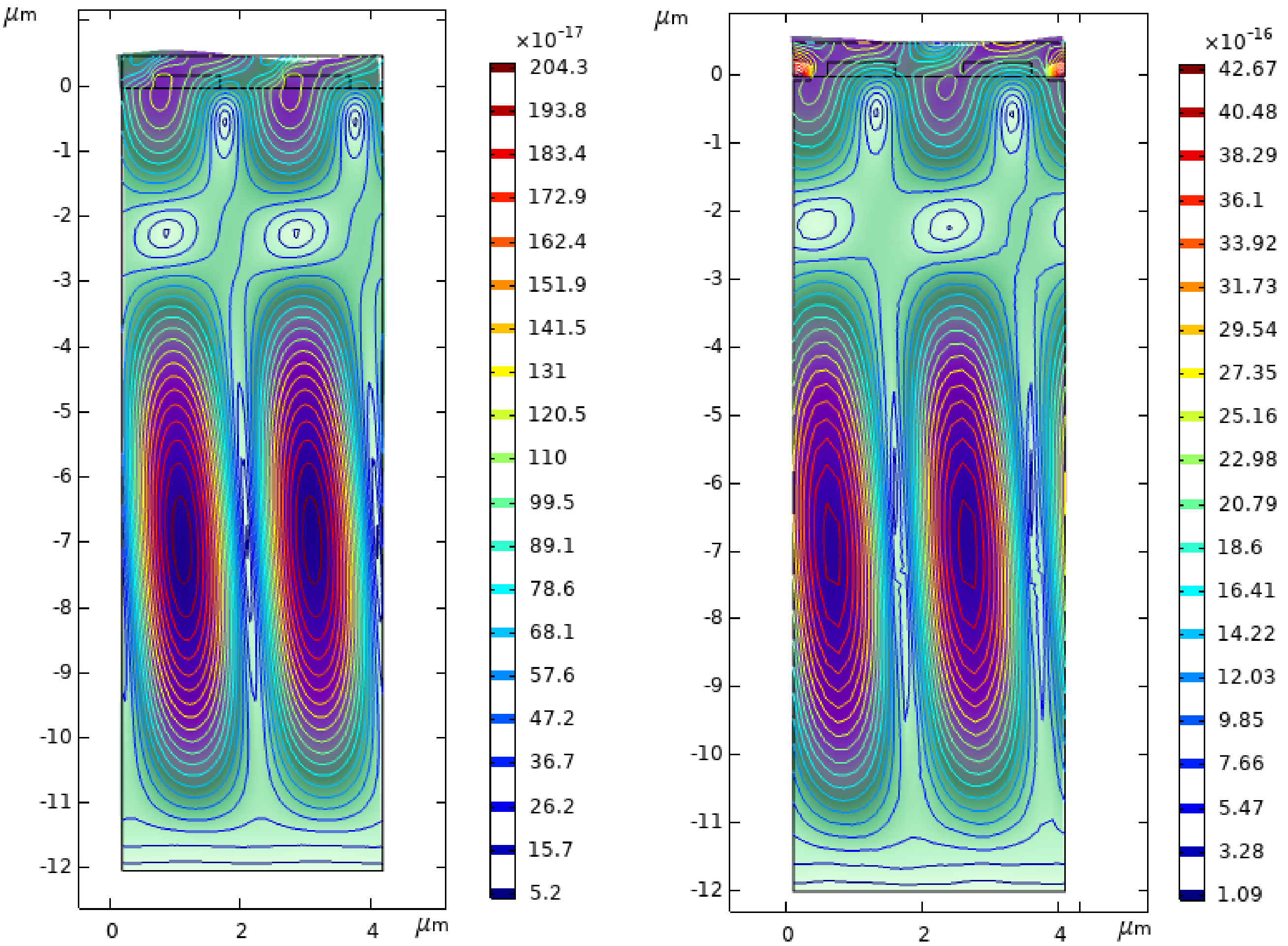


Figure 10: Mode 4 of solid mechanics.

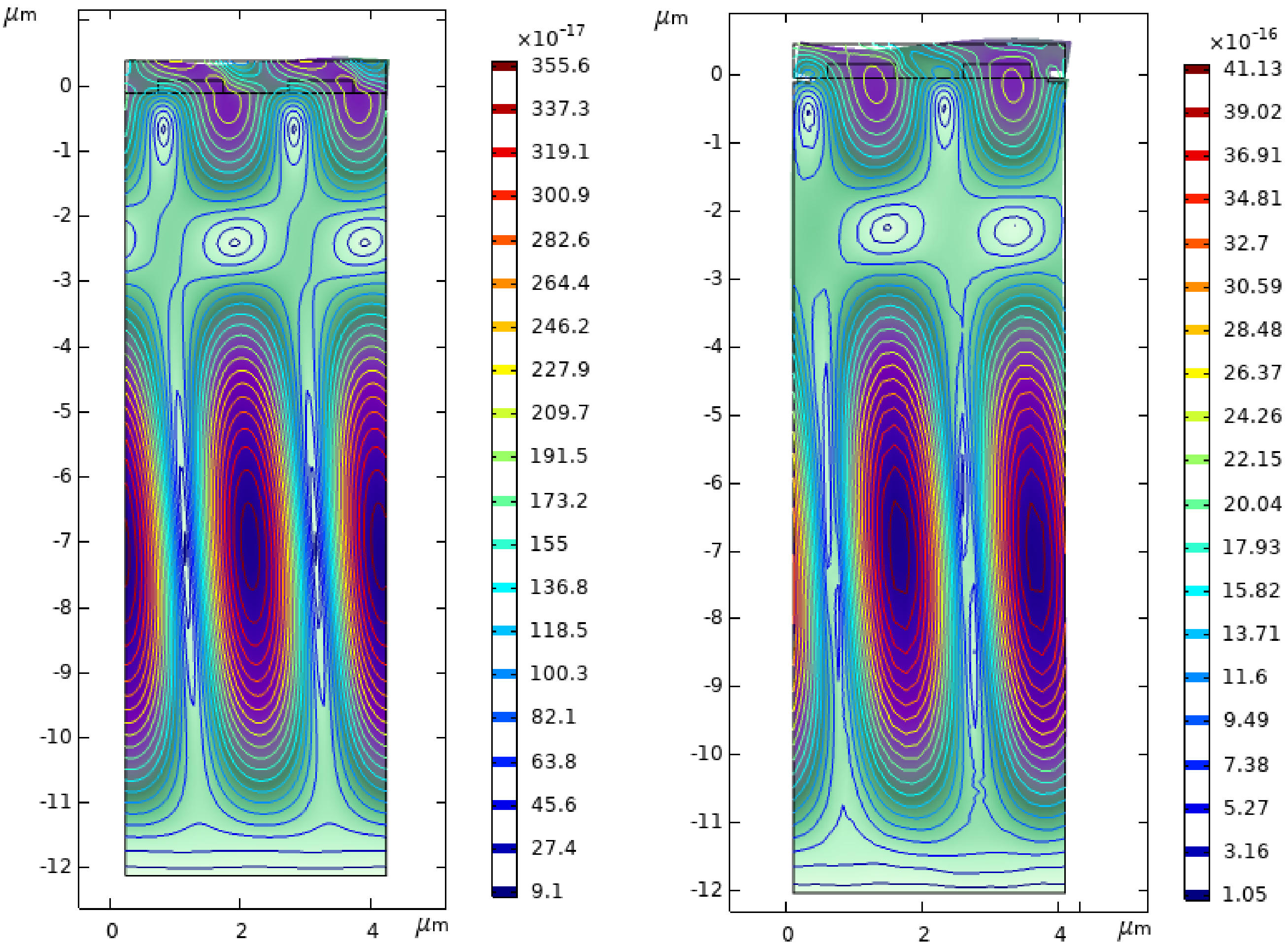


Figure 11: Mode 5 of solid mechanics.

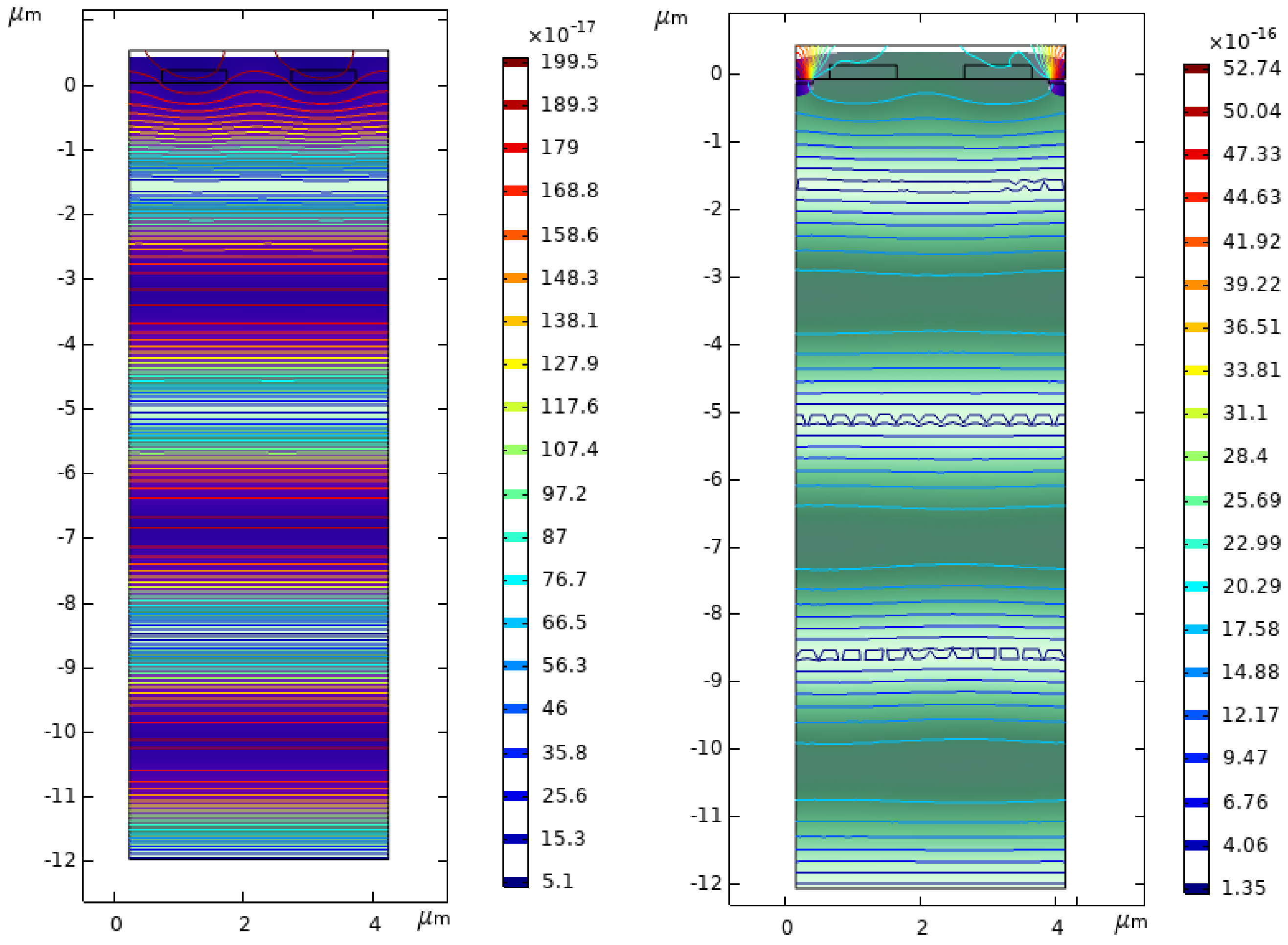


Figure 12: Mode 6 of solid mechanics.

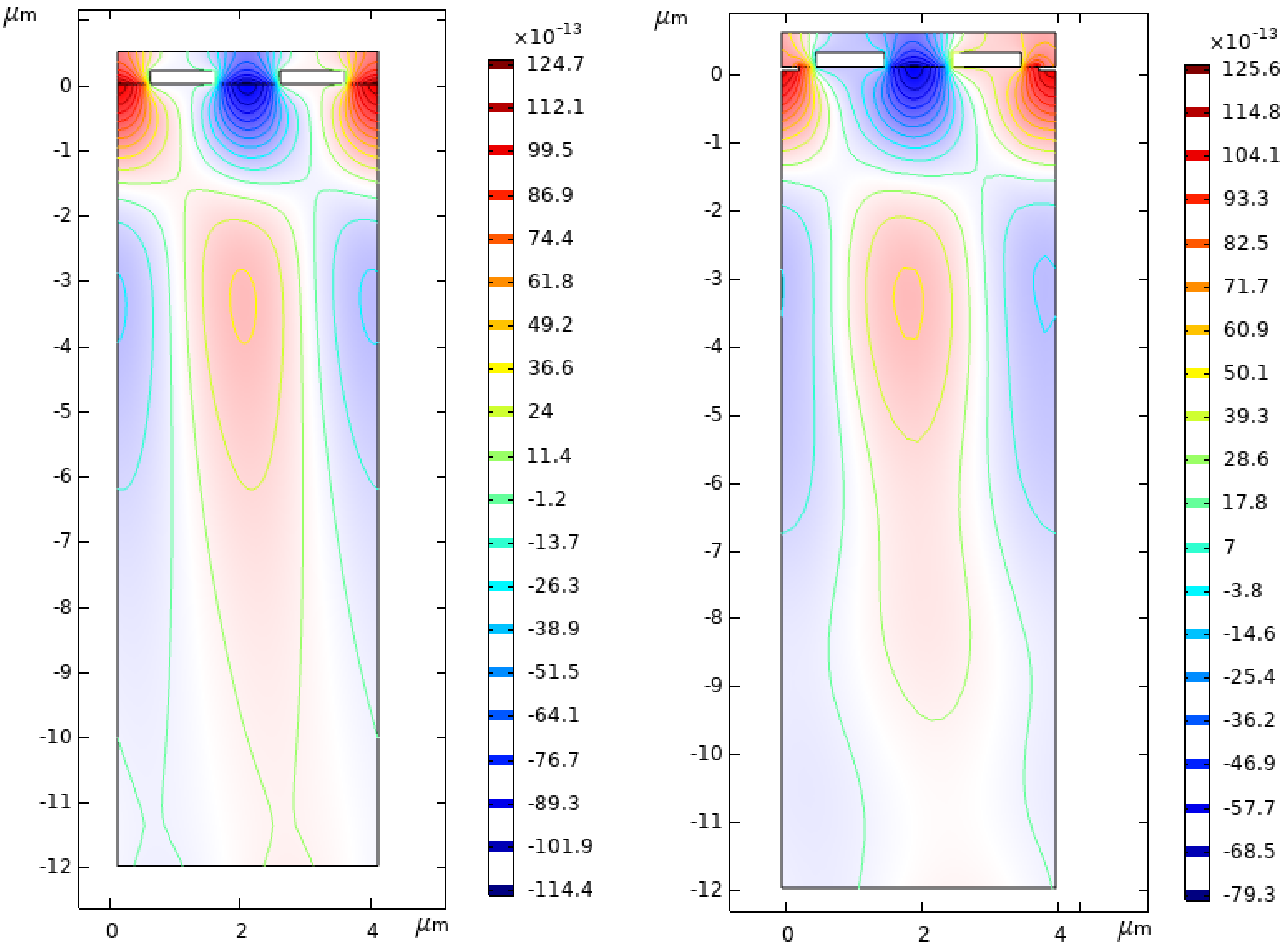


Figure 13: Mode 1 of electric potential.

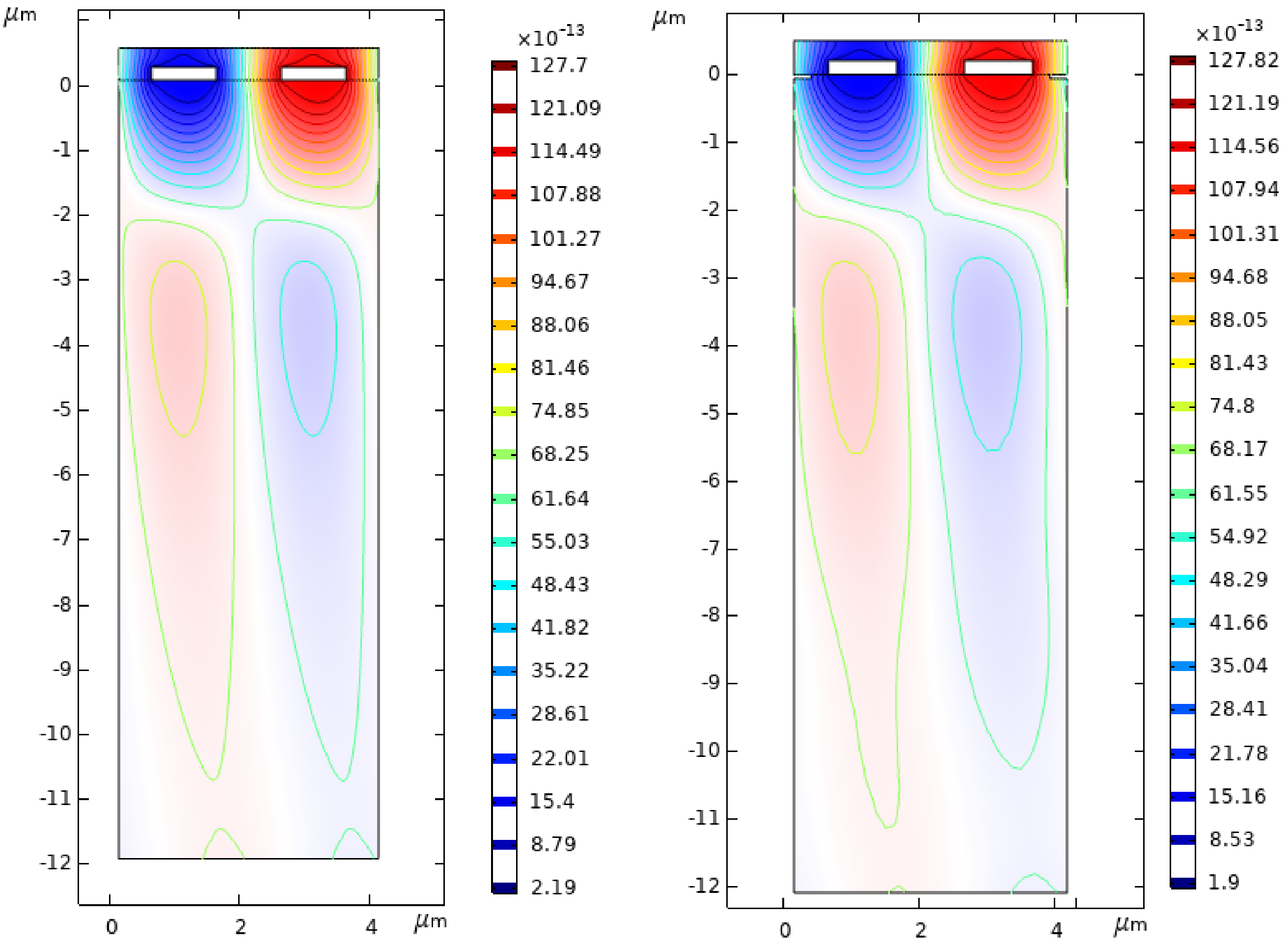


Figure 14: Mode 2 of electric potential.

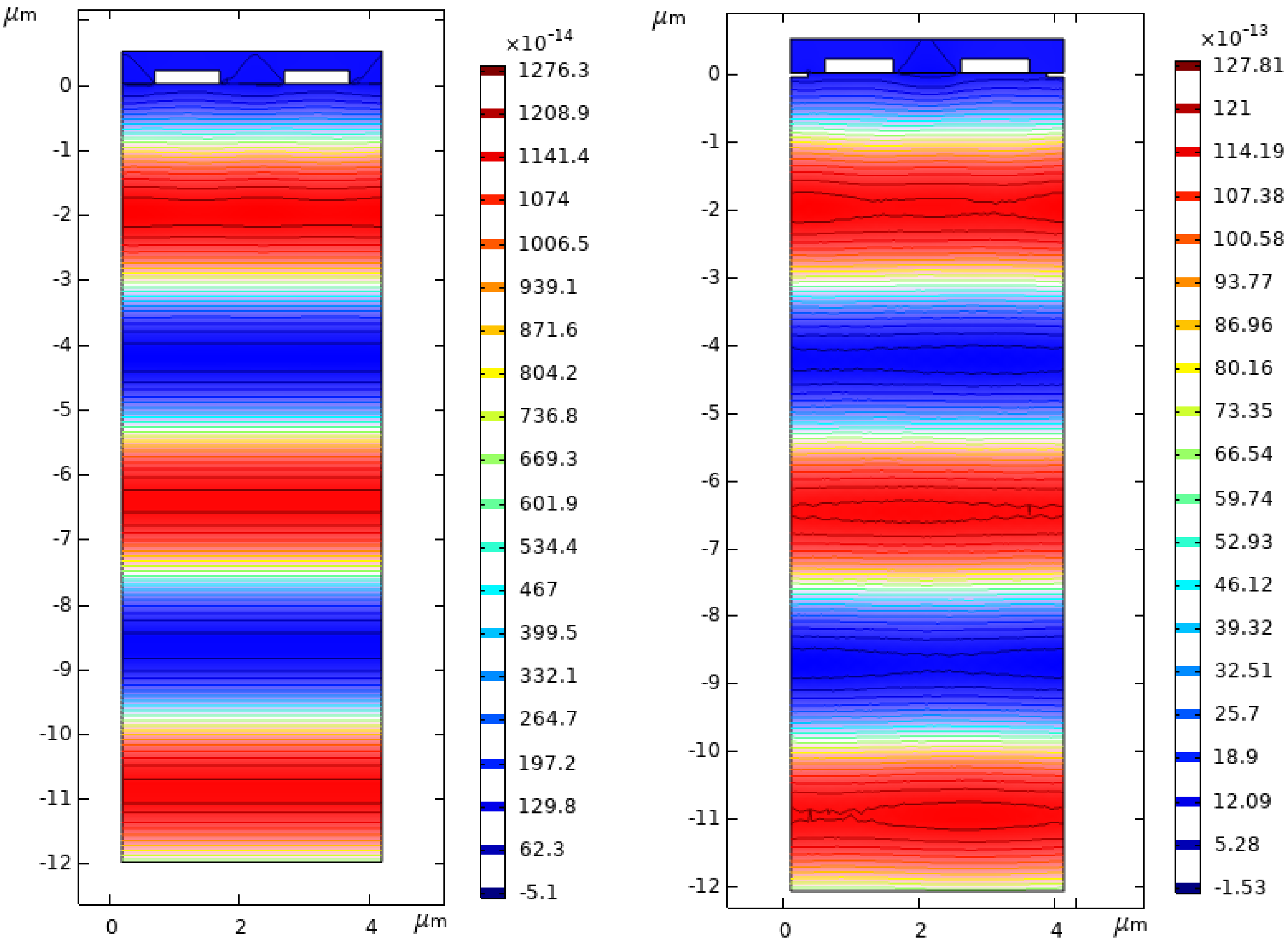


Figure 15: Mode 3 of electric potential.

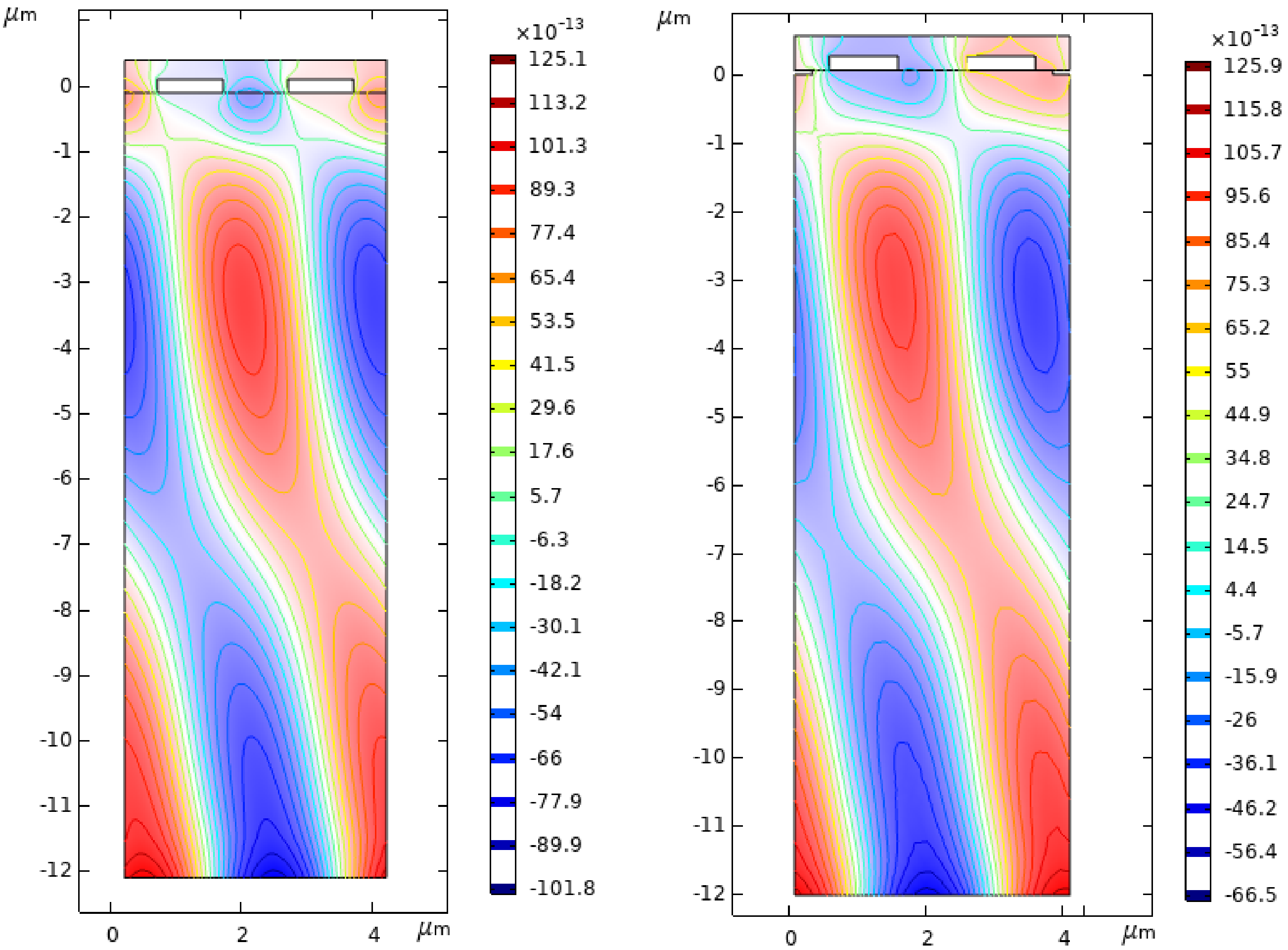


Figure 16: Mode 4 of electric potential.

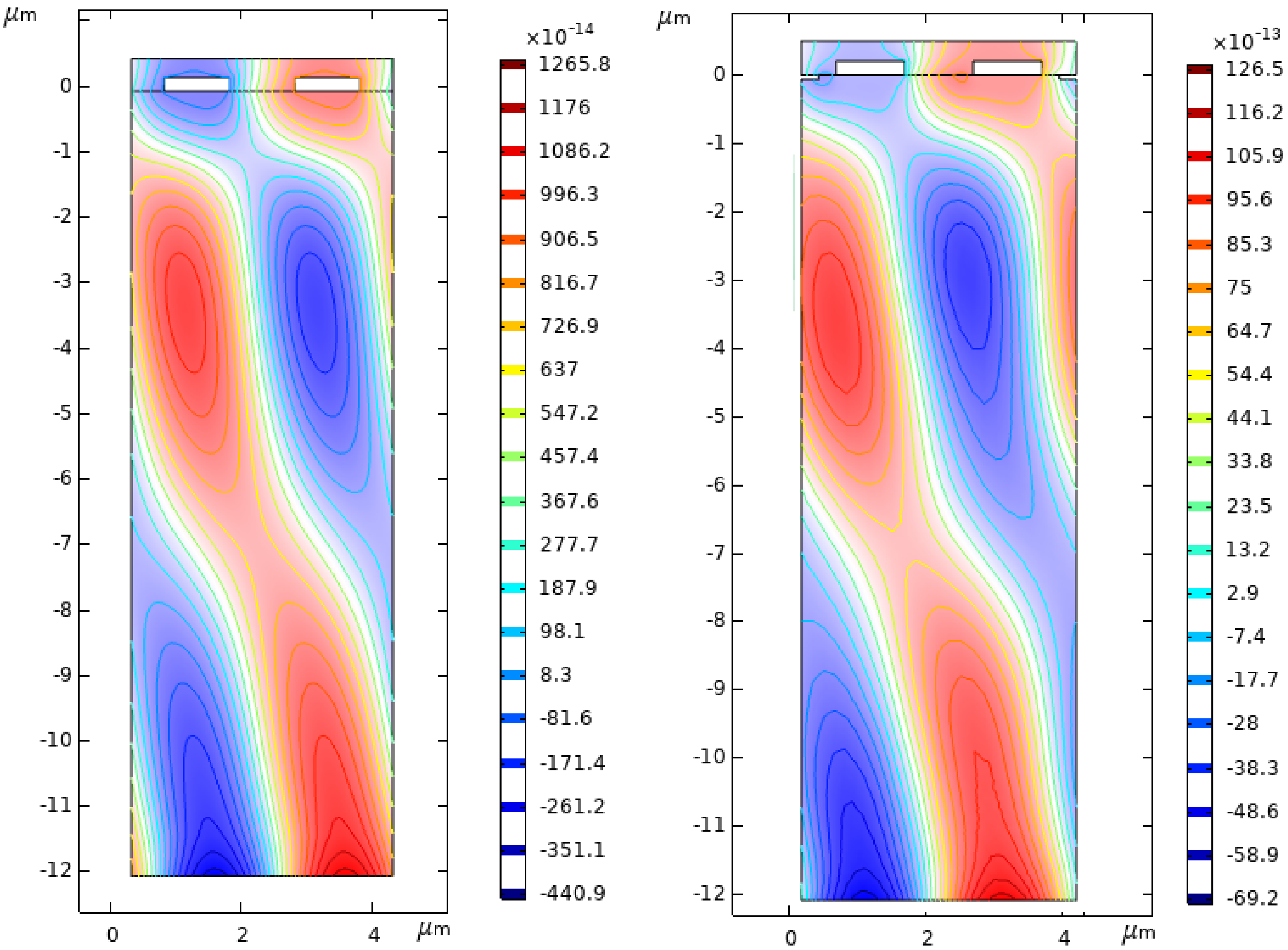


Figure 17: Mode 5 of electric potential.

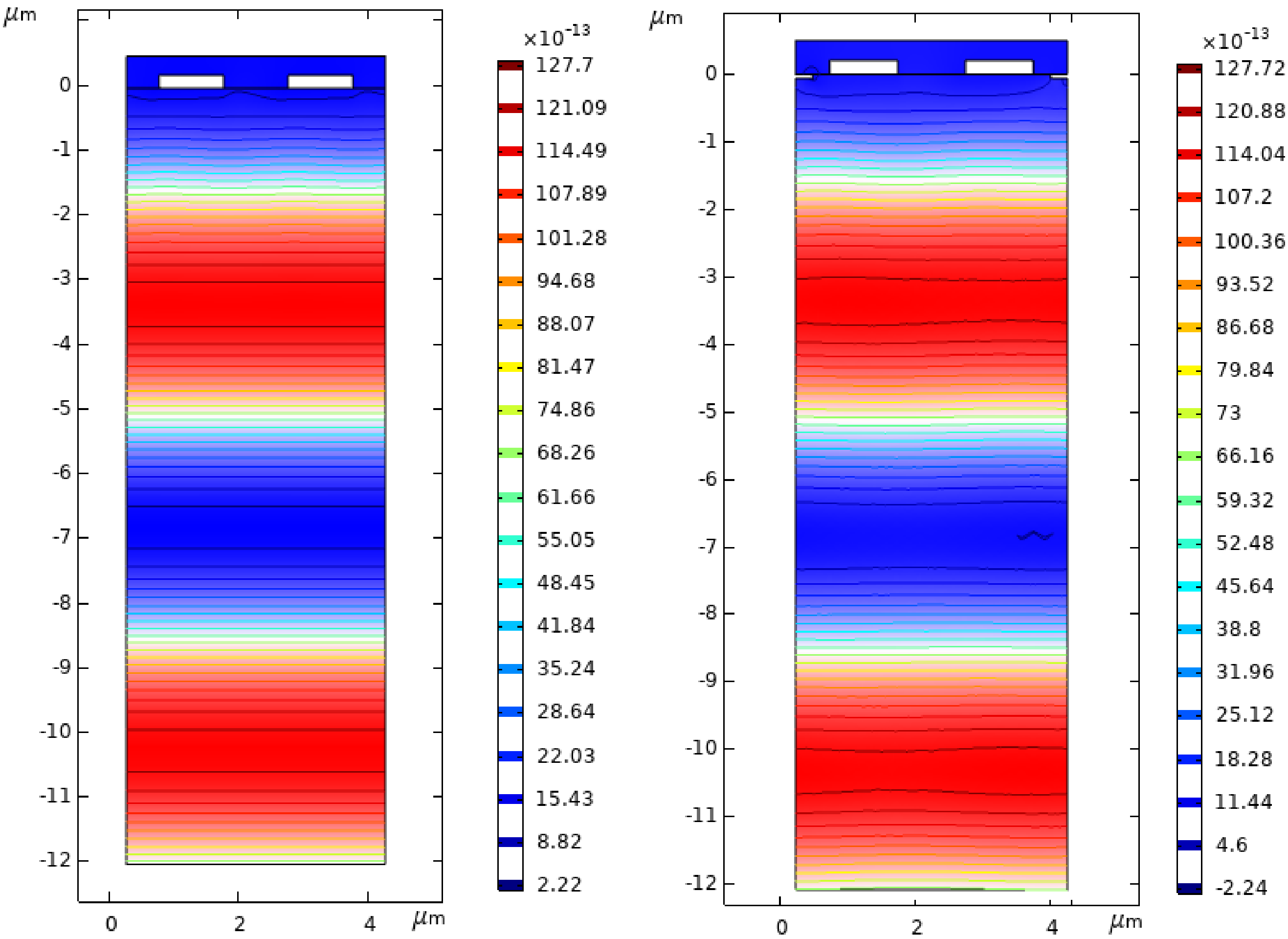


Figure 18: Mode 6 of electric potential.

profundity of engendering of the Rayleigh waves, and its vibration vitality quickly diminishes with expanding profundity. At the point when the profundity of the Rayleigh waves spread is near one to two frequencies, the abundancy of the molecule is as of now little. Mode transformation will happen when sound waves engender to various media, including various materials and breaks.

In the previous not many years another class of SAW gadgets has been a work in progress dependent on the utilization of one port SAW resonators as lumped components with their impedance firmly changing in a recurrence scope of compelling SAW excitation. These 'SAW impedance components' can be associated in stepping stool type, adjusted scaffold type, or others kinds of systems to give wanted channel qualities. Fig. 5 shows the Deformed shape plot of the antiresonance SAW mode. In the Fig. 5 induction attributes of a solitary component are broke down utilizing coupling of mode (COM) model reenactments. It is discovered that thunderous sort attributes of a long transducer can be depicted by extremely straightforward recipes.

The current case resonate at their own resonance frequency and their vibrations couple to the acoustic mode of the SAW resonator. Fig. **??** shows the Deformed shape plot of the resonation SAW mode.

Fig. 2 shows the Electric potential dispersal and misshapenings at antiresonance, antisymmetric with respect to the point of convergence of each cathode.

Fig. 7 shows the Mode 1 of solid mechanics. The essential detecting, in the SAW sensor, is the aftereffect of a move in the working recurrence because of stacking of the polymer film by the consumed gas atoms. The SAW sensor gadgets are normally intended to run at RF (radio frequencies, in the scope of several MHz). To gauge the recurrence deviation because of gas spongy, the framework introduced with square chart in Fig. 7 will be utilized. Here, the SAW sensor chip is made out of two SAW gadgets created on a similar substrate in CMOS innovation, where one gadget is covered with a gas spongy polymer also, the subsequent one is fixed to fill in as a kind of perspective recurrence source.

Fig. 8 shows the Mode 2 of solid mechanics. In surface-wave tweet channels, the waveform v(t) to be inspected is itself a twitter waveform. Examining is almost constantly done in synchronism with the waveform, that is, at relating focuses in each cycle.An antisymmetric mode has inverse wave amplitudes in the two tracks, and this gives zero anode voltages.Fig. 9 shows the Mode 3 of solid mechanics. Through this figure the gadget input is coupled to the yield. The general structure has two waveguide modes, symmetric and antisymmetric, which give the gadget a two-post recurrence reaction. This gadget can give a surprisingly little partial data transmission, in the locale of 1 percent. It is additionally exceptionally little truly, a significant factor for portable telephone handsets. Fig. 10 shows the Mode 4 of solid mechanics. At high frequencies Td and Ld are enormous, and for the most reduced speed arrangements they are seen as nonexistent. For this situation, the left half of eq. (2.40) approaches solidarity. Correlation shows that the speed draws near the Rayleigh-wave speed, VR. In this manner the two Lamb modes, one symmetric what's more, one antisymmetric, each become identical to a Rayleigh wave on the upper surface in addition to a Rayleigh wave on the lower surface. Fig. 11 shows the Mode 5 of solid mechanics. The most reduced request mode (the one with littlest stage speed) is symmetric, what's more, ensuing modes switch back and forth among antisymmetric and symmetric. At zero recurrence, the main mode has stage speed v01, the plane-wave speed of the 'quick' locale. Fig. 12 shows the Mode 6 of solid mechanics.Different modes have this speed at their cutoff frequencies.

System portrayed in above is utilized to ascertain inclusion misfortune. First the charge circulation was determined. In control dissemination figuring semi static estimation is utilized. In this count edge impacts has been disregarded. Truth be told edge impact is insignificant for IDT's with in excess of 10 sets of finger. The finger thickness is accepted exceptionally little contrast with the frequency, in this way the mass stacking impact of fingers has been disregarded. For this figuring the test SAW speed and recreated coupling coefficient has been utilized. Fig. 13 shows the Mode 1 of electric potential.

The physical nature of the strips isn't indicated here, yet as a rule they will be shorted metal anodes. Then again, grooves are regularly utilized in resonators, and opencircuit (disengaged) terminals are likewise conceivable. The physical idea of the waves isn't indicated now, however it is accepted that the wavefronts are corresponding to the strips and that just one wave mode is included. At first, we accept power protection, however misfortunes will be viewed as later. Fig. 14 shows the Mode 2 of electric potential.

Fig. 15 shows the Mode 3 of electric potential. Truly, the suspicion of limited reflection coefficients may not be very right. For instance, the conduct of a metal anode in a surface-wave grinding relies upon the setup of a few neighboring anodes in light of coupling because of the electric fields. For open-circuit anodes, a wave occurrence on one terminal incites fields reaching out more than a few neighbors, so the reflection component isn't confined to the area of one cathode.

Fig. 16 shows the Mode 4 of electric potential. This framework can be depicted by coupled-mode conditions identified with those of Fig. 15, however created to take into consideration variety the y course as well as the x course. Utilizing the standard limit conditions prompts a convoluted scattering connection with numerous arrangements.

Fig. 17 shows the Mode 5 of electric potential. Fig. 17 shows the permission of a one-port resonator, utilizing with COManalysis for the gratings and transducers. The little waves about 0.7MHz from the principle top are because of extra pitifully coupled full modes. The pinnacle recurrence for Y is the reverberation recurrence, and $ImY$ is zero at the antiresonance recurrence.

Fig. 18 shows the Mode 6 of electric potential. As appeared in Fig. 18 the proportional circuit is taken to have an arrangement branch of impedance with an equal part of impedance on each side. The circuit is proportional as in its Y-lattice is equivalent to that of the surface-wave gadget. The arrangement branch has impedance , spoke to by a thunderous circuit with motional inductance Lm. To discover this, we can overlook misfortunes by setting

## 4 Conclusion

In this paper decreasing the temperature of surface acoustic wave resonator at specific frequencies which is an important challenge for electronic designers was investigated. Various modifications of the cooling in ZnO based sensitive element for the two-port surface acoustic wave sensor (SAW) design were considered. The effect of microchannel for cooling in SAW sensor characteristics was investigated by finite element simulation method. Obtained versatile flexible multiparameter model allowed the evaluation of performance parameters. The optimal parameters for SAW sensor design could be estimated by the proposed approach.

## 5 References

1. K. Ho, E. R. Lindgren, K. S. Rawlinson, L. K. McGrath, and J. L. Wright, "Development of a Surface Acoustic Wave Sensor for In-Situ Monitoring of Volatile Organic Compounds," Sensors vol. 3, pp. 236–247, 2003.
2. S. Ahmadi, F. Hassani, C. Korman, M. Rahaman, and M. Zaghloul, "Characterization of Multi- and Single-layer Structure SAW Sensor," Sensors 2004, Proceedings of IEEE, vol. 3, pp. 1129–1132, 2004.
3. Campbell C. K. (1998). Surface Acoustic Wave Devices for Mobile and Wireless Communication. San Diego:

Academic Press.
4. Tengjiao Jiang, Chunlei Li ,Qiang Han ,Surface acoustic waves in 2D-phononic crystal of laminated pillars on a semi-infinite ZnO substrate , Physics Letters A, Volume 383, Issue 33, 28, 2019, 125956
5. R. Baumgartner, B. Reuth, W. Lanz, K. Petterson "Partial Discharge-Part IX: PD in Gas-insulated Substations-Fundamental considerations" IEEE Electr Insul. Mag., 7 (1997), pp. 5-13

6. G. Eranna, B.C. Joshi, D.P. Runthala, R.P. Gupta Oxide Materials for Development of Integrated Gas Sensors—A Comprehensive Review Critical Reviews in Solid State and Materials Sciences, 29 (3–4) (2004), pp. 111-188

7. Monika Chaudhary, Amita Gupta Microcantilever-based Sensors Defence Science Journal, 59 (6) (2009), pp. 634-641

8. S. Iijima Helical microtubules of graphitic carbon Nature, 354 (1991), p. 56

9. R. Quintero, F. Simonetti, P. Howard, J. Friecll, A. Sellinger Noncontact laser ultrasonic inspection of ceramic matrix composites (CMCs) NDT E Int., 88 (2017), pp. 8-16

10. N. Hosoya, R. Umino, A. Kanda, I. Kajiwara, A. Yoshinaga Lamb wave generation using nanosecond laser ablation to detect damage J. Vib. Control, 24 (24) (2017), pp. 5842-5853

11. M.I. Chen, S.P. Tesng, P.Y. Lo, C.H. Yang Characterization of wedge waves propagating along wedge tips with defects Ultrasonics, 82 (2018), pp. 289-297

12. Y. Wang, D. Chen, C. Wu, J. Xie Effect of droplet boundary behaviors on SAW attenuation for potential microfluidic applications Jpn. J. Appl. Phys., 58 (3) (2019), p. 037001

13. X.Y. Du, Y.Q. Fu, J.K. Luo, A.J. Flewitt, W.I. Milne Microfluidic pumps employing surface acoustic waves generated in ZnO thin films J. Appl. Phys., 105 (2) (2009), p. 024508

14. Y.Q. Fu, L. Garcia-Gancedo, H.F. Pang, S. Porro, Y.W. Gu, J.K. Luo, X.T. Zu, F. Placido, J.I.B. Wilson, A.J. Flewitt, W.I. Milne Microfluidics based on ZnO/nanocrystalline diamond surface acoustic wave devices Biomicrofluidics, 6 (2) (2012), p. 024105

15. Y. Wang, Z. Xu, Y. Wang, J. Xie A study on AIN film-based SAW attenuation in liquids and their potential as liquid ethanol sensors Sensors, 17 (8) (2017), p. 1813

16. M. Abdelgawad, S.L. Freire, H. Yang, A.R. Wheeler All-terrain droplet actuation Lab Chip, 8 (5) (2008), pp. 672-677